17

Modeling Dynamic Friction

17.1 INTRODUCTION

Early research was focused on bearings that operate under steady conditions, such as constant load and velocity. Since the traditional objectives of tribology were prevention of wear and minimizing friction-energy losses in steady-speed machinery, it is understandable that only a limited amount of research effort was directed to time-variable velocity. However, steady friction is only one aspect in a wider discipline of friction under time-variable conditions. Variable friction under unsteady conditions is referred to as *dynamic friction*. There are many applications involving dynamic friction, such as friction between the piston and sleeve in engines where the sliding speed and load periodically vary with time.

In the last decade, there was an increasing interest in dynamic friction as well as its modeling. This interest is motivated by the requirement to simulate dynamic effects such as friction-induced vibrations and stick-slip friction. In addition, there is a relatively new application for dynamic friction models—improving the precision of motion in control systems.

It is commonly recognized that friction limits the precision of motion. For example, if one tries to drag a heavy table on a rough floor, it would be impossible to obtain a high-precision displacement of a few micrometers. In fact, the minimum motion of the table will be a few millimeters. The reason for a low-precision motion is the negative slope of friction versus velocity. In comparison,

one can move an object on well-lubricated, slippery surfaces and obtain much better precision of motion.

In a similar way, friction limits the precision of motion in open-loop and closed-loop control systems. This is because the friction has nonlinear characteristics of negative slope of friction versus velocity and discontinuity at velocity reversals. Friction causes errors of displacement from the desired target (hang-off) and instability, such as a stick-slip friction at low velocity.

There is an increasing requirement for ultrahigh-precision motion in applications such as manufacturing, precise measurement, and even surgery. Hydrostatic or magnetic bearings can minimize friction; also, vibrations are used to reduce friction (dither). These methods are expensive and may not be always feasible in machines or control systems.

An alternate approach that is still in development is model-based friction compensation. The concept is to include a friction model in the control algorithm. The control is designed to generate continuous on-line timely torque by the servomotor, in the opposite direction to the actual friction in the mechanical system. In this way, it is possible to approximately cancel the adverse effects of friction. Increasing computer capabilities make this method more and more attractive. This method requires a dynamic friction model for predicting the friction under dynamic conditions.

There is already experimental verification that displacement and velocity errors caused by friction can be substantially reduced by friction compensation. This effect has been demonstrated in laboratory experiments; see Amin et al. (1997). Friction compensation has been already applied successfully in actual machines. For example, Tafazoli (1995) describes a simple friction compensation method that improves the precision of motion in an industrial machine.

Another application of dynamic friction models is the simulation of friction-induced vibration (stick-slip friction). The simulation is required for design purposes to prevent these vibrations.

Stick-slip friction is considered a major limitation for high-precision manufacturing. In addition to machine tools, stick-slip friction is a major problem in measurement devices and other precision machines. A lot of research has been done to eliminate the stick-slip friction, particularly in machine tools. Some solutions involve hardware modifications that have already been discussed. These are expensive solutions that are not feasible in all cases. Attempts were made to reduce the stick-slip friction by using high-viscosity lubricant that improves the damping, but this would increase the viscous friction losses. Moreover, high-viscosity oil results in a thicker hydrodynamic film that reduces the precision of the machine tool. This undesirable effect is referred to as *excessive float*.

Various methods have been tried by several investigators to improve the stability of motion in the presence of friction. However, a model-based approach has the potential to offer a relatively low-cost solution to this important problem.

Armstrong-Hélouvry (1991) summarized the early work in friction modeling of the Stribeck curve by empirical equations. Also, Dahl (1968) introduced a model to describe the presliding displacement during stiction. However, these models are "static," in the sense that the friction is represented by an instantaneous function of sliding velocity and load. In recent years, several empirical equations were suggested to describe the phase lag and hysteresis in dynamic friction. Hess and Soom (1990) and Dupont and Dunlap (1993) developed such models.

17.2 DYNAMIC FRICTION MODEL FOR JOURNAL BEARINGS*

Harnoy and Friedland (1994) suggested a different modeling approach for lubricated surfaces, based on the physical principles of hydrodynamics. In the following section, this model is compared to friction measurements. This approach is based on the following two assumptions:

1. The load capacity, in the boundary and mixed lubrication regions, is the sum of a contact force (elastic reaction between the surface asperities) and hydrodynamic load capacity.
2. The friction has two components: a solid component due to adhesion in the asperity contacts and a viscous shear component.

This modeling approach was extended to line-contact friction by Rachoor and Harnoy (1996). Polycarpou and Soom (1995, 1996) and Zhai et al. (1997) extended this approach and derived a more accurate analysis for the complex elastohydrodynamic lubrication of line contact.

Under steady-state conditions of constant sliding velocity, the friction coefficient of lubricated surfaces is a function of the velocity. However, under dynamic conditions, when the relative velocity varies with time, such as oscillatory motion or motion of constant acceleration, the instantaneous friction depends not only on the velocity at that instant but is also a function of the velocity history.

The existence of dynamic effects in friction was recognized by several investigators. Hess and Soom (1995, 1996) observed a hysteresis effect in oscillatory friction of lubricated surfaces. They offered a model based on the steady f–U curve with a correction accounting for the phase lag between friction and velocity oscillations. The magnitude of the phase lag was determined empirically. A time lag between oscillating friction and velocity in lubricated

*This and subsequent sections in this chapter are for advanced studies.

surfaces was observed and measured earlier. It is interesting to note that Rabinowicz (1951) observed a friction lag even in dry contacts.

The following analysis offers a theoretical model, based on the physical phenomena of lubricated surfaces, that can capture the primary effect and simulate the dynamic friction. The result of the analysis is a dynamic model, expressed by a set of differential equations, that relates the force of friction to the time-variable velocity of the sliding surfaces. A model that can predict dynamic friction is very useful as an enhancement of the technology of precise motion control in machinery. For control purposes, we want to find the friction at oscillating low velocities near zero velocity.

Under classical hydrodynamic lubrication theory, (see Chapters 4–7) the fluid film thickness increases with velocity. The region of a full hydrodynamic lubrication in the f–U curve (Fig. 16-1) occurs when the sliding velocity is above the transition velocity, U_{tr} required to generate a lubrication film thicker than the size of the surface asperities. In Fig. 16-1, U_{tr} is the velocity corresponding to the minimum friction. In the full hydrodynamic region, there is only viscous friction that increases with velocity, because the shear rates and shear stresses are proportional to the sliding velocity.

Below the transition velocity, U_{tr}, the Stribeck curve shows the mixed lubrication region where the thickness of the lubrication film is less than the maximum size of the surface asperities. Under load, there is a contact between the surfaces, resulting in elastic as well as plastic deformation of the asperities. In the mixed region, the external load is carried partly by the pressure of the hydrodynamic fluid film and partly by the mechanical elastic reaction of the deformed asperities. The film thickness increases with velocity; therefore, as the velocity increases, a larger part of the external load is carried by the fluid film. The result is that the friction decreases with velocity in the mixed region, because the fluid viscous friction is lower than the mechanical friction at the contact between the asperities.

This discussion shows that the friction force is dependent primarily on the lubrication film thickness, which in turn is an increasing function of the steady velocity. However, for time-variable velocity, the relation between film thickness and velocity is much more complex. The following analysis of unsteady velocity attempts to capture the physical phenomena when the lubrication film undergoes changes owing to a variable sliding velocity. As a result of the damping in the system and the mass of the sliding body, there is a time delay to reach the film thickness that would otherwise be generated under steady velocity.

17.3 DEVELOPMENT OF THE MODEL

Consider a hydrodynamic journal bearing under steady conditions, when all the variables, such as external load and speed, are constant with time. Under these

steady conditions, the journal center O_1 does not move relative to the bearing sleeve, and the friction force remains constant. In practice, these steady conditions will come about after a transient interval for damping of any initial motion of the journal center. When there is a motion of the journal center O_1, however, the oil film thickness and the friction force are not constant, which explains the dynamic effects of unsteady friction.

Before proceeding with the development of the dynamic model, the model for steady friction in the mixed lubrication region is presented. Dubois and Ocvirk (1953) derived the equations for full hydrodynamic lubrication of a short bearing. The following is an extension of this analysis to the mixed lubrication region. In the mixed region there is direct contact between the surface asperities combined with hydrodynamic load capacity. The theory is for a short journal bearing, because it is widely used in machinery, and because the steady performance of a short bearing in the full hydrodynamic region is already well understood and can be described by closed-form equations.

The mixed lubrication region is where the hydrodynamic minimum film thickness, h_n, is below a certain small transition magnitude, h_{tr}. Under load, the asperities are subject to elastic as well as plastic deformation due to the high-pressure contact at the tip of the asperities. Although the load is distributed unevenly between the asperities, the average elastic part of the deformation is described by the elastic recoverable displacement, δ, of the surfaces toward each other, in the direction normal to the contact area. The reaction force between the asperities of the two surfaces is an increasing function of the elastic, recoverable part of the deformation, δ. The normal reaction force of the asperities as a function of δ is similar to that of a spring; however, this springlike behavior is not linear.

In a journal bearing in the mixed lubrication region, the average normal elastic deformation, δ of the asperities is proportional to the difference between the transition minimum film thickness, h_{tr}, and the actual lower minimum film thickness, h_n:

$$\delta = h_{\text{tr}} - h_n \tag{17-1}$$

The elastic reaction force, W_e, of the asperities is similar to that of a nonlinear spring:

$$W_e = k_n(\delta)\,\delta \tag{17-2}$$

where $k_n(\delta)$ is the stiffness function of the asperities to elastic deformation in the direction normal to the surface. The contact areas between the asperities increase with the load and deformation δ. Therefore, $k_n(\delta)$ is an increasing function of δ.

If the elastic reaction force, W_e, between the asperities is approximated by a contact between two spheres, Hertz theory indicates that the reaction force, W_e, is proportional to $\delta^{3/2}$:

$$W_e \propto \delta^{3/2} \tag{17-3}$$

and Eq. (17-2) becomes

$$W_e = k_n \delta \;\Rightarrow\; k_n = k_0 \delta^{1/2} \tag{17-4}$$

Here, k_0 is a constant which depends on the geometry and the elastic modulus of the two materials in contact. In fact, an average asperity contact is not identical to that between two spheres, and a better modeling precision can be obtained by determining empirically the two constants, k_0 and n, in the following expression for the normal stiffness:

$$k_n = k_0 \delta^n \tag{17-5}$$

The two constants are selected for each material combination to give the best fit to the steady Stribeck curve in the mixed lubrication region.

For a journal bearing, the average elastic reaction of surface asperities in the mixed region, W_e in Eq. (17-2), can be expressed in terms of the eccentricity ratio, $\varepsilon = e/C$. In addition, a transition eccentricity ratio, ε_{tr}, is defined as the eccentricity ratio at the point of steady transition from mixed to hydrodynamic lubrication (in tests under steady conditions). This transition point is where the friction is minimal in the steady Stribeck curve.

The elastic deformation, δ (average normal asperity deformation), in Eq. (17-1) at the mixed lubrication region can be expressed in terms of the difference between ε and ε_{tr}:

$$\delta = C(\varepsilon - \varepsilon_{tr}) \tag{17-6}$$

and the expression for the average elastic reaction of the asperities in terms of the eccentricity ratio is

$$W_e = \kappa_n(\varepsilon)(\varepsilon - \varepsilon_{tr})\Delta \tag{17-7}$$

The elastic reaction force, W_e, is only in the mixed region, where the difference between ε and ε_{tr} is positive. For this purpose, the notation Δ is defined as

$$\Delta = \begin{cases} 1 & \text{if } (\varepsilon - \varepsilon_{tr}) > 0 \\ 0 & \text{if } (\varepsilon - \varepsilon_{tr}) \le 0 \end{cases} \tag{17-8}$$

In a similar way to Eq. (17-5), $\kappa_n(\varepsilon)$ is a normal stiffness function, but it is a function of the difference of ε and ε_{tr},

$$\kappa_n(\varepsilon) = \kappa_0(\varepsilon - \varepsilon_{tr})^n \tag{17-9}$$

In the case of a spherical asperity, $n = 0.5$ and κ_0 is a constant. In actual contacts, the magnitude of the two constants n and κ_0 is determined for the best fit to the steady (Stribeck) f–U curve. In Eq. (17-7), $\Delta = 0$ in the full hydrodynamic region, and the elastic reaction force W_e, is also zero. But in the mixed region, $\Delta = 1$, and the elastic reaction force W_e is an increasing function of the eccentricity ratio ε.

In the mixed region, the total load capacity vector $\vec{W}$ of the bearing is a vector summation of the elastic reaction of the asperities, $\vec{W}_e$ and the hydrodynamic fluid film force, $\vec{W}_h$:

$$\vec{W} = \vec{W}_e + \vec{W}_h \tag{17-10}$$

The bearing friction force, F_f, in the tangential direction is the sum of contact and viscous friction forces. The contact friction force is assumed to follow Coulomb's law; hence, it is proportional to the normal contact load, W_e, while the hydrodynamic, viscous friction force follows the short bearing equation; see Eq. (7-27). Also, it is assumed that the asperities, in the mixed region, do not have an appreciable effect on the hydrodynamic performance.

Under these assumptions, the equation for the total friction force between the journal and sleeve of a short journal bearing over the complete range of boundary, mixed, and hydrodynamic regions is

$$F_f = f_m \kappa_n(\varepsilon)\, C(\varepsilon - \varepsilon_{\text{tr}})\Delta\, sgn(U) + \frac{LR\mu}{C^2}\, \frac{2\pi}{(1-\varepsilon^2)^{0.5}}\, U \tag{17-11}$$

Here, f_m is the static friction coefficient, L and R are the length and radius of the bearing, respectively, C is the radial clearance, and μ is the lubricant viscosity. The friction coefficient of the bearing, f, is a ratio of the friction force and the external load, $f = F_f/F$. The symbol sgn(U) means that the contact friction is in the direction of the velocity U.

17.4 MODELING FRICTION AT STEADY VELOCITY

The load capacity is the sum of the hydrodynamic force and the elastic reaction force. The equations for the hydrodynamic load capacity components of a short journal bearing [Eq. (7–16)] were derived by Dubois and Ocvirk, 1953. The

following equations extend this solution to include the hydrodynamic components and the elastic reaction force:

$$F\cos(\phi-\pi)=\kappa_n(\varepsilon)\,C\,(\varepsilon-\varepsilon_{\text{tr}})\Delta+\frac{\varepsilon^2}{(1-\varepsilon^2)^2}\,\frac{\mu L^3}{C^2}\,|U| \tag{17-12}$$

$$F\sin(\phi-\pi)=\frac{\pi\varepsilon^2}{(1-\varepsilon^2)^2}\,\frac{\mu L^3}{C^2}\,U \tag{17-13}$$

The coordinates ϕ and e (Fig. 15-1) describe the location of the journal center in polar coordinates. The direction of the elastic reaction W_e is in the direction of X. In Eq. (17-12), the external load component F_x is equal to the sum of the hydrodynamic force component due to the fluid film pressure and the elastic reaction W_e, at the point of minimum film thickness. In Eq. (17-13), the load component F_y is equal only to the hydrodynamic reaction, because there is no contact force in the direction of Y.

For any steady velocity U in the mixed region, ($\varepsilon > \varepsilon_{\text{tr}}$) and for specified C, L, F, μ and $\kappa_n(\varepsilon)$, Eqs. (17-12 and 17-13) can be solved for the two unknowns, ϕ and ε. Once the relative eccentricity, ε, is known, the friction force F_f can be calculated from Eq. (17-11), and the bearing friction coefficient, f, can be obtained for specified R and f_m. By this procedure, the Stribeck curve can be plotted for the mixed and hydrodynamic regions.

For numerical solution, there is an advantage in having Eqs. (17-12) and (17-13) in a dimensionless form. These equations can be converted to dimensionless form by introducing the following dimensionless variables:

$$\overline{U}=\frac{U}{U_{\text{tr}}};\qquad \overline{F}=\frac{C^2}{\mu U_{\text{tr}}L^3}\,F;\qquad \overline{\kappa}=\frac{C^3}{\mu U_{\text{tr}}L^3}\,\kappa_n \tag{17-14}$$

Here $\overline{\kappa}$ is a dimensionless normal stiffness to deformation at the asperity contact. The deformation is in the direction normal to the contact area. The velocity U_{tr} is at the transition from mixed to hydrodynamic lubrication (at the point of minimum friction in the f–U chart). The dimensionless form of Eqs. (17-12) and (17-13) is

$$\overline{F}\cos(\phi-\pi)=\overline{\kappa}(\varepsilon)(\varepsilon-\varepsilon_{\text{tr}})\Delta-0.5J_{12}\varepsilon\,|\,\overline{U}\,| \tag{17-15}$$

$$\overline{F}\sin(\phi-\pi)=0.5J_{11}\varepsilon\,\overline{U} \tag{17-16}$$

The integrals J_{11} and J_{12} are defined in Eqs. (7-13). Equations (17-15) and (17-16) apply to the mixed as well as the hydrodynamic lubrication regions in the Stribeck curve.

17.5 MODELING DYNAMIC FRICTION

For the purpose of developing the dynamic friction model, the existing hydrodynamic short bearing theory of Dubois and Ocvirk is extended to include the mixed region and dynamic conditions.

The assumptions of hydrodynamic theory of steady short bearings are extended to dynamic conditions. The pressure gradients in the x direction (around the bearing) are neglected, because they are very small in comparison with the gradients in the z (axial) direction (for directions, see Fig. 7-1). Similar to the analysis of a steady short bearing (see Chapter 7), only the pressure wave in the region $0 < \theta < \pi$ is considered for the fluid film force calculations. In this region, the fluid film pressure is higher than atmospheric pressure. In addition, the conventional assumptions of Reynolds' classical hydrodynamic theory are maintained. The viscosity, μ, is assumed to be constant (at an equivalent average temperature). The effects of fluid inertia are neglected, but the journal mass is considered, for it is of higher order of magnitude than the fluid mass.

Recall that under dynamic conditions the equations of motion are (see Chapter 15)

$$\vec{F} - \vec{W} = m\vec{a} \tag{17-17}$$

Writing Eq. (17-17) in components in the direction of W_x and W_y (i.e., the radial and tangential directions in Fig. 15-1), the following two equations are obtained in dimensionless terms:

$$\overline{F}_x - \overline{W}_x = \overline{m}\ddot{\varepsilon} - \overline{m}\varepsilon\dot{\phi}^2 \tag{17-18}$$

$$\overline{F}_y - \overline{W}_y = -\overline{m}\varepsilon\ddot{\phi} - 2\overline{m}\dot{\varepsilon}\dot{\phi}, \tag{17-19}$$

where the dimensionless mass and force are defined, respectively, as

$$\overline{m} = \frac{C^3}{\mu L^3 R^2}\, m; \qquad \overline{F} = \frac{C^2}{\mu U_{tr} L^3}\, F \tag{17-20}$$

Under dynamic conditions, the equations for the hydrodynamic load capacity components of a short journal bearing are as derived in Chapter 15. These equations are used here; in this case, however, the velocity is normalized by the transition velocity, U_{tr}. In a similar way to steady velocity, the load capacity components are due to the hydrodynamic pressure and elastic reaction force

$$\overline{W}_x = \overline{\kappa}(\varepsilon)(\varepsilon - \varepsilon_{tr})\Delta - 0.5J_{12}\varepsilon \mid \overline{U} \mid + J_{12}\varepsilon\dot{\phi} + J_{22}\dot{\varepsilon} \tag{17-21}$$

$$\overline{W}_y = 0.5\varepsilon J_{11}\overline{U} - J_{11}\varepsilon\dot{\phi} - J_{12}\dot{\varepsilon} \tag{17-22}$$

Substituting these hydrodynamic and reaction force in Eqs. (17-18) and (17-19) yields

$$\overline{F}(t)\cos(\phi-\pi)=\overline{\kappa}(\varepsilon-\varepsilon_{tr})\Delta-0.5\varepsilon J_{12}|\overline{U}|+J_{12}\varepsilon\dot{\phi}+J_{22}\dot{\varepsilon}+\overline{m}\ddot{\varepsilon}-\overline{m}\dot{\phi}^{2} \tag{17-23}$$

$$\overline{F}(t)\sin(\phi-\pi)=0.5\varepsilon J_{11}\overline{U}-J_{11}\varepsilon\dot{\phi}-J_{12}\dot{\varepsilon}-\overline{m}\varepsilon\ddot{\phi}-2\overline{m}\dot{\varepsilon}\dot{\phi} \tag{17-24}$$

Here $\overline{F}(t)$ is a time-dependent dimensionless force acting on the bearing. The magnitude of this external force, as well as its direction is a function of time. In the two equations, ε is the eccentricity ratio, ϕ is defined in Fig. 15-1, and $\overline{m}$ is dimensionless mass, defined by Eq. (17-20). The definition of the integrals J_{ij} and their solutions are in Eqs. (7-13).

Equations (17-23) and (17-24) are two differential equations, which are required for the solution of the two time-dependent functions ε and ϕ. The solution of the two equations for ε and ϕ as a function of time allows the plotting of the trajectory of the journal center O_1 *in polar coordinates*.

These two differential equations yield the time-variable $\varepsilon(t)$, which in turn can be substituted into Eq. (17-11) for the computation of the friction force. For numerical computations, it is convenient to use the following dimensionless equation for the friction force obtained from Eq. (17-11):

$$\overline{F}_f=f_m\,\overline{\kappa}(\varepsilon)\,C\,(\varepsilon-\varepsilon_{tr})\,\Delta\,sgn(\overline{U})+\frac{RC}{L^2}\,\frac{2\pi}{(1-\varepsilon^2)^{0.5}}\,\overline{U} \tag{17-25}$$

The dimensionless friction force and velocity are defined in Eq. (17-14). The friction coefficient of the bearing is the ratio of the dimensionless friction force and external load:

$$f=\frac{\overline{F}_f}{\overline{F}} \tag{17-26}$$

The set of three equations (17-23), (17-24) and (17-25) represents the dynamic friction model. For any time-variable shaft velocity $U(t)$ and time-variable load, the friction coefficient can be solved as a function of time or velocity.

This model can be extended to different sliding surface contacts, including EHD line and point contacts as well as rolling-element bearings. This can be done by replacing the equations for the hydrodynamic force of a short journal bearing with that of a point contact or rolling contact. These equations are already known from elastohydrodynamic lubrication theory; see Chapter 12.

17.6 COMPARISON OF MODEL SIMULATIONS AND EXPERIMENTS

Dynamic friction measurements were performed with the four-bearing measurement apparatus, which was described in Sec. 14.7. A computer with on-line data-acquisition system was used for plotting the results and analysis.

The model coefficients are required for comparing model simulations and experimental f–U curves under dynamic conditions. The modeling approach is to determine the model coefficients from the steady Stribeck curve. Later, the model coefficients are used to determine the characteristics under dynamic conditions.

In order to simplify the comparison, Eq. (17-25) has been modified and the coefficient γ introduced to replace a combination of several constants:

$$\overline{F}_f = f_m\,\overline{\kappa}(\varepsilon)\,C\,(\varepsilon - \varepsilon_{\text{tr}})\,\Delta\,sgn(\overline{U}) + \gamma\,\frac{2\pi}{(1-\varepsilon^2)^{0.5}}\,\overline{U} \tag{17-27}$$

Here, f_m is the stiction friction coefficient and γ is a bearing geometrical coefficient. The friction force has two components: The first term is the contact component due to asperity interaction, and the second term is the viscous shear component. The normal stiffness constant, k_0, is selected by iterations to result in the best fit with the Stribeck curve in the mixed region.

A few examples are presented of measured curves of a test bearing (Table 17-1) as compared to theoretical simulations. The experiments were conducted under constant load and oscillating sliding velocity.

Friction measurements for bidirectional sinusoidal velocity were conducted under loads of 104 N and 84 N for each of the four test sleeve bearings. The analytical model was simulated for the following periodic velocity oscillations:

$$U = 0.127\sin(\omega t) \tag{17-28}$$

Here, ω is the frequency (rad/s) of sliding velocity oscillations and U is the sliding velocity of the journal surface. The four-bearing apparatus was used to measure the dynamic friction between the shaft and the four sleeve bearings. Multigrade oil was applied, because the viscosity is less sensitive to variations of temperature, but it still varied initially by dissipation of friction energy during the

TABLE 17-1 Data from Friction Measurement Apparatus

Diameter of bearing ($D = 2R$)	$D = 0.0254$ m
Length of bearing	$L = 0.019$ m
Radial clearance in bearing	$C = 0.05$ mm
Mass of journal	$m = 2.27$ kg
Bearing material	Brass
Oil	SAE 10W-40

TABLE 17-2 Model Parameters for a Load of 84 N

$f_m = 0.26$	$k_0 = 7.5 \times 10^5$	$\mu = 0.02$ N-s/m^2
$U_{tr} = 0.06$ m/s	$F = 104$ N	$C = 5.08e^{-5}$ m
$\varepsilon_{tr} = 0.9727$	$m = 2.27$ kg	$\gamma = 0.0011$

test. After several cycles, however, a steady state was reached in which repeatability of the experiments was sustained.

For each bearing load, the Stribeck curve was initially produced by our four-bearing testing apparatus and used to determine the optimal coefficients required for the dynamic model in Eqs. (17-23), (17-24), and (17-27). The stiction friction coefficient, f_m and velocity at the transition, U_{tr}, were taken directly from the experimental steady Stribeck curve. The geometrical coefficient, γ, was determined from the slope in the hydrodynamic region, while the coefficient k_0 was determined to obtain an optimal fit to the experimental Stribeck curve in the mixed region. All other coefficients in Table 17-2, such as viscosity and bearing dimensions, are known. These constant coefficients, determined from the steady f–U curve, were used later for the simulation of the following f–U curves under dynamic conditions.

17.6.1 Bearing Load of 104 N (Table 17-2, Figs. 17-1, 17-2, 17-3)

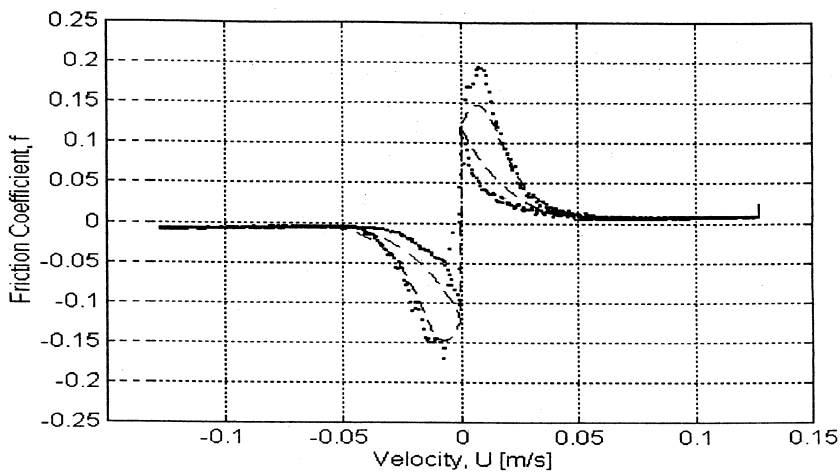

FIG. 17-1 Comparison of measured and theoretical f–U curves for sinusoidal sliding velocity: load = 104 N, $U = 0.127 \sin(0.045t)$ m/s, oscillation frequency = 0.045 rad/s (measurement . . . , simulation —).

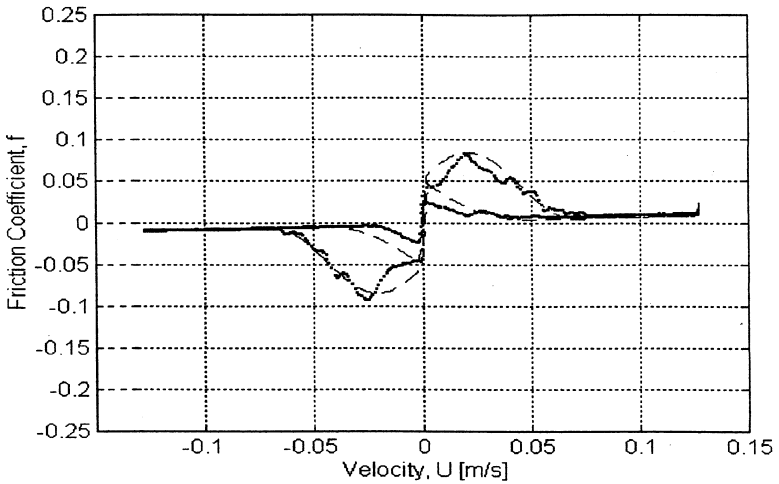

FIG. 17-2 Comparison of measured and theoretical f–U curves for sinusoidal sliding velocity: load = 104 N, $U = 0.127\sin(0.25t)$ m/s, oscillation frequency = 0.25 rad/s (measurement . . . , simulation —).

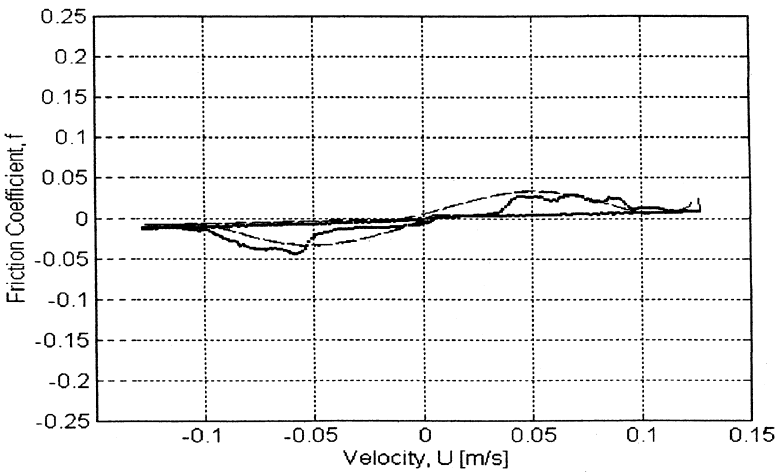

FIG. 17-3 Comparison of measured and theoretical f–U curves for sinusoidal sliding velocity: load = 104 N, $U = 0.127\sin(t)$ m/s, oscillation frequency = 1 rad/s (measurement . . . , simulation —).

17.6.2 Bearing Under Load of 84 N (Table 17-3, Figs. 17-4, 17-5, 17-6)

TABLE 17-3 Model Parameters for a Load of 84 N

$f_m = 0.26$	$k_0 = 6.25 \times 10^5$	$\mu = 0.02$ N-s/m^2
$U_{tr} = 0.05$ m/s	$F = 84$ N	$C = 5.08e^{-5}$ m
$\varepsilon_{tr} = 0.9718$	$m = 2.27$ kg	$\gamma = 0.0011$

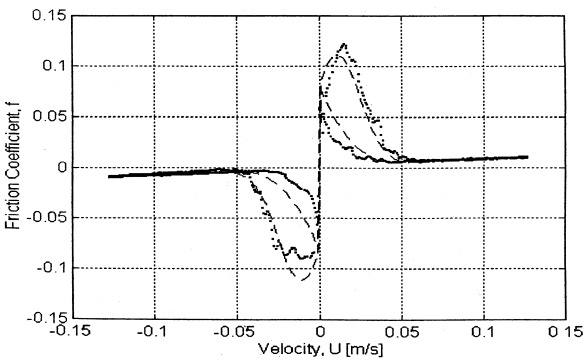

FIG. 17-4 Comparison of measured and theoretical f–U curves for sinusoidal sliding velocity: load = 84 N, $U = 0.127 \sin(0.1t)$ m/s, oscillation frequency = 0.1 rad/s (measurement . . . , simulation —).

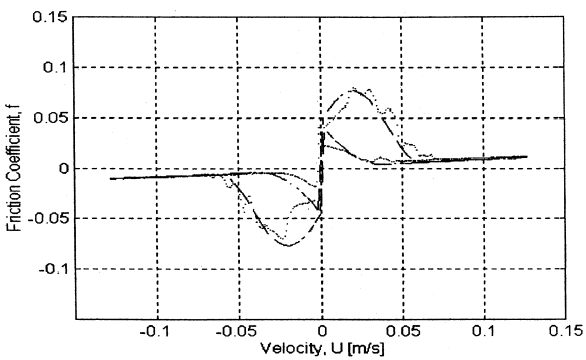

FIG. 17-5 Comparison of measured and theoretical f–U curves for sinusoidal sliding velocity: load = 84 N, $U = 0.127 \sin(0.25t)$ m/s, oscillation frequency = 0.25 rad/s (measurement . . . , simulation —).

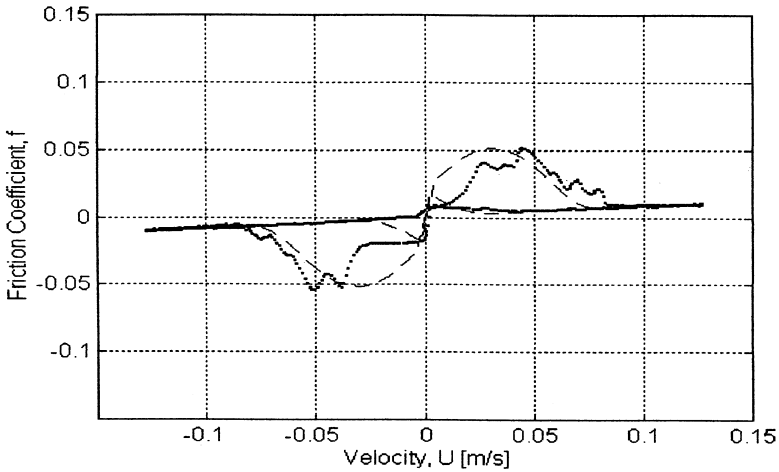

FIG. 17-6 Comparison of measured and theoretical f–U curves for sinusoidal sliding velocity: load = 84 N, $U = 0.127 \sin(0.5t)$ m/s, oscillation frequency = 0.5 rad/s (measurement . . . , simulation —).

17.6.3 Conclusions

In conclusion, the f–U curves indicate reasonable agreement between experiments and simulation. At low frequency of velocity oscillations, the curves reduce to the steady Stribeck curve and do not demonstrate any significant hysteresis. At higher frequency, both analytical and experimental curves display similar hysteresis characteristics, which increase with the frequency. This phenomenon was detected earlier in experiments of unidirectional velocity oscillations.

In addition to the hysteresis, the experiments, as well as the simulation, detected several new dynamic friction characteristics that are unique to bidirectional oscillations with velocity reversals.

1. The magnitude of the friction discontinuity (and stiction friction) at zero velocity reduces when the oscillation frequency increases.
2. The stiction friction reduces to zero above a certain frequency of velocity oscillations.
3. The discontinuity at velocity reversals in the experimental curves is in the form of a vertical line. This means that the Dahl effect (presliding displacement) in journal bearings is relatively small, because the discontinuity is an inclined line wherever presliding displacement is of higher value.

The explanation for the reduction in the magnitude of the stiction force at higher frequencies is as follows: At high frequency there is insufficient time for the fluid film to be squeezed out. As the frequency increases, the fluid film is thicker, resulting in lower stiction force at velocity reversals.